Atmospheric
Measurement
Techniques
Discussions

Open Access

Hygroscopic growth of atmospheric aerosol particles based on active remote sensing and radiosounding measurements

M. J. Granados-Muñoz[1,2], F. Navas-Guzmán[1,2,*], J. A. Bravo-Aranda[1,2], J. L. Guerrero-Rascado[1,2], H. Lyamani[1,2], A. Valenzuela[1,2], G. Titos[1,2], J. Fernández-Gálvez[1,2], and L. Alados-Arboledas[1,2]

[1]Dpt. Applied Physics, Faculty of Sciences, University of Granada, Fuentenueva s/n, 18071, Granada, Spain
[2]Andalusian Institute for Earth System Research (IISTA-CEAMA), Avda. del Mediterráneo s/n, 18006, Granada, Spain
[*]now at: Institute of Applied Physics (IAP), University of Bern, Bern, Switzerland

Title Page

Abstract	Introduction
Conclusions	References
Tables	Figures

|◄ | ►|
◄ | ►
Back | Close

Full Screen / Esc

Printer-friendly Version

Interactive Discussion

Aerosol hygroscopic growth by active remote sensing and radiosoundings

M. J. Granados-Muñoz et al.

Abstract

A new methodology based on combining active and passive remote sensing and simultaneous and collocated radiosounding data to study the aerosol hygroscopic growth effects on the particle optical and microphysical properties is presented. The identification of hygroscopic growth situations combines the analysis of multiespectral aerosol particle backscatter coefficient and particle linear depolarization ratio with thermodynamic profiling of the atmospheric column. We analysed the hygroscopic growth effects on aerosol properties, namely the aerosol particle backscatter coefficient and the volume concentration profiles, using data gathered at Granada EARLINET station. Two study case, corresponding to different aerosol loads and different aerosol types, are used for illustrating the potential of this methodology. Values of the aerosol particle backscatter coefficient enhancement factors range from 2.10 ± 0.06 to 3.90 ± 0.03, being similar to those previously reported in the literature. Differences in the enhancement factor are directly linked to the composition of the atmospheric aerosol. The largest value of the aerosol particle backscatter coefficient enhancement factor corresponds to the presence of sulphate and marine particles that are more affected by hygroscopic growth. On the contrary, the lowest value of the enhancement factor corresponds to an aerosol mixture containing sulphates and slight traces of mineral dust. The Hänel parameterization is applied to these case studies, obtaining results within the range of values reported in previous studies, with values of the γ exponent of 0.56 ± 0.01 (for anthropogenic particles slightly influenced by mineral dust) and 1.07 ± 0.01 (for the situation dominated by anthropogenic particles), showing the convenience of this remote sensing approach for the study of hygroscopic effects of the atmospheric aerosol under ambient unperturbed conditions. For the first time, the retrieval of the volume concentration profiles for these cases using the Lidar Radiometer Inversion Code (LIRIC) allows us to analyse the aerosol hygroscopic growth effects on aerosol volume concentration, observing a stronger increase of the fine mode volume concentration with increasing relative humidity.

Title Page

Abstract	Introduction
Conclusions	References
Tables	Figures

|◄   ►|

◄   ►

Back   Close

Full Screen / Esc

Printer-friendly Version

Interactive Discussion

1 Introduction

The influence of atmospheric aerosols in the Earth's climate is still affected by a high uncertainty. Scientific knowledge on the interaction between atmospheric aerosol and solar radiation is quite low compared to other atmospheric constituents mainly due to atmospheric aerosol high spatio-temporal variability (IPCC, 2013). As it is well known, atmospheric aerosol can affect the Earth–Atmosphere energy budget by means of direct effects (by scattering or absorbing solar radiation) and indirect effects (mainly by changes in cloud properties). Therefore, changes in aerosol properties can highly influence the Earth's climate. Aerosol particles size may increase due to water uptake (hygroscopic growth) altering their size distribution and their associated optical and microphysical properties under high relative humidity conditions. Therefore, hygroscopic growth affects the direct scattering of radiation (Hänel, 1976; Hegg et al., 1993) and especially the indirect effects, as the affinity of atmospheric aerosols for water vapor is highly related to their ability to act as cloud condensation nuclei (CCN) (Charlson et al., 1992; Feingold and Morley, 2003).

In the past years there has been an increasing interest in the hygroscopic growth effects on the aerosol optical and microphysical properties and many studies have already been performed (e. g. Veselovskii et al., 2009; Zieger et al., 2013; Titos et al., 2014a, c). Much of the recent research was performed by means of humidified nephelometers (Covert et al., 1972; Fierz-Schmidhauser et al., 2010a, and references therein) or humidified tandem differential mobility analysers (Massling et al., 2007; Wu et al., 2013, and references therein). Nonetheless, these instruments present two main problems. Firstly, due to experimental set-up limitations it is difficult to provide accurate results above RH of 85 % (Wulfmeyer and Feingold, 2000). Secondly, they modify the ambient conditions by drying the air sample and then humidifying it again up to a certain value of RH, altering thus the aerosol properties and being also subject to aerosol losses in the sampling lines.

Title Page

Abstract | Introduction

Conclusions | References

Tables | Figures

|◄ | ►|

◄ | ►

Back | Close

Full Screen / Esc

Printer-friendly Version

Interactive Discussion

Opposite to in-situ measurements, lidar systems present the main advantage that they can provide vertically resolved measurements without modifying the aerosol sample or its surroundings. They also detect RH close to saturation, which is of great importance since the range between 85 and 100 % RH is where particles are more affected by hygroscopic growth (Feingold and Morley, 2003). Therefore, lidar systems are adequate to provide useful information about aerosol hygroscopic properties if favourable atmospheric conditions occur. However, they present the major drawback that the sample and conditions are not controlled in anyway and the number of cases with adequate conditions is usually low compared to in-situ measurements. In the past years, some studies have already been performed by using lidar systems to detect aerosol hygroscopic growth with promising results (Ferrare et al., 1998; Wulfmeyer and Feingold, 2000; Feingold and Morley, 2003; Veselovskii et al., 2009; DiGirolamo et al., 2013). However, many of these studies present the major drawback that experimental RH profiles were not available and assumptions were made to obtain RH data (Wulfmeyer and Feingold, 2000; Feingold and Morley, 2003; Feingold et al., 2006; Pahlow et al., 2006). In some other cases, RH profiles were taken from quite distant radiosounding measurements (Veselovskii et al., 2009). The availability of collocated radiosounding data allows the reduction of assumptions needed. In this study, a methodology to study aerosol hygroscopic growth based on lidar data and collocated radiosounding RH profiles is presented and applied at Granada EARLINET (European Aerosol Research Lidar Network) experimental site in order to study aerosol hygroscopic growth under unperturbed ambient conditions.

2 Experimental site and instrumentation

This study was performed at the Andalusian Institute for Earth System Research, IISTA-CEAMA, located in Granada (37.16° N, 3.61° W, 680 m a.s.l.). The station is described in more detail in (Lyamani et al., 2010; Titos et al., 2012; Valenzuela et al., 2012). Granada is affected by continental climate conditions. Temperature presents

M. J. Granados-Muñoz et al.

large seasonal variations, with cool winters and hot summers, and a strong diurnal thermal oscillation (up to 20 °C), which lead to strong RH variations along the day. Seasonal variations in RH are also quite important with mean monthly values ranging between 41 % in summer and 76 % in winter (source: State Meterological Agency, www.aemet.es). An analysis of RH profiles based on measurements of water vapour mixing ratio from Raman lidar and temperature from microwave radiometry for one-year period, performed for 500 m-layers at different altitudes revealed that over Granada the 60 % of the data present RH values in the range between 20 and 60 %, whereas only 25 % of these layers present values larger than 60 % (Navas-Guzmán et al., 2014).

Due to its proximity to the African continent, the experimental site is usually affected by mineral dust events (Valenzuela et al., 2012), reaching altitudes of up to 5500 m a.s.l. (Guerrero-Rascado et al., 2008, 2009; Navas-Guzmán et al., 2013). In addition, Europe acts as an important source of anthropogenic pollution (Lyamani et al., 2006a, b). The experimental site is also affected by local and regional sources. In a recent source apportionment study of fine and coarse particulate matter at surface level, Titos et al. (2014b) pointed out that the major aerosol sources at Granada are road traffic (dominated by diesel engines) and mineral dust as well as fuel-based domestic heating during winter time. The levels of mineral matter increase considerably from winter to summer due to the dryness conditions, which favour re-suspension processes and the higher frequency of Saharan outbreaks. Traffic related sources increase its contribution during winter compared with summer (Titos et al., 2014b) as a consequence of higher emissions and lower mixing layer heights (Granados-Muñoz et al., 2012).

The experimental station is equipped with a multiwavelength Raman lidar system model LR331D400 (Raymetrics S.A.). Such instrument, called MULHACEN, is described in detail in Guerrero-Rascado et al. (2008, 2009). The lidar system emits at 355, 532 and 1064 nm. The detection system records the elastic signals at these three wavelengths and Raman signals in three additional channels: 387 and 607 nm, corresponding to the nitrogen Raman channel, and 408 nm, corresponding to water vapour Raman channel. In addition, the perpendicular and parallel components of the visible

channel are detected, allowing us to study the depolarization properties of the atmospheric aerosol. Uncertainties associated to the elastic lidar signals are around 15 %, considering the statistical uncertainties retrieved with Monte Carlo techniques according to Pappalardo et al. (2004) and Guerrero-Rascado et al. (2008). The Raman lidar is part of EARLINET (Pappalardo et al., 2014). It has been part of the EARLINET-ASOS (European Aerosol Research Lidar Network – Advanced Sustainable Observation System) project and currently is included in the ACTRIS (Aerosols, Clouds, and Trace gases Research InfraStructure Network) European project.

In addition, the radiometric station is equipped with a sun photometer CIMEL CE-318-4. The sun photometer provides column-integrated atmospheric aerosol properties. The automatic tracking sun and sky scanning radiometer makes sun direct measurements with a 1.2° full field of view every 15 min at 340, 380, 440, 500, 675, 870, 940 and 1020 nm (nominal wavelengths). These solar extinction measurements are used to compute aerosol optical depth (τ_λ) at each wavelength except for the 940 nm channel, which is used to retrieve total column water vapour (or precipitable water). The estimated uncertainty in computed τ_λ, due primarily to calibration uncertainty, is around 0.010–0.021 for field instruments (which is spectrally dependent, with the higher errors in the UV) (Eck et al., 1999). The sun photometer located in Granada is included in the AERONET network (Holben et al., 1998). The AERONET Version 2 Level 1.5 data are used in this study for the characterization of the aerosol properties and for the retrieval of the aerosol microphysical properties profiles in combination with backscattered elastic lidar signals by means of the Lidar Radiometer Inversion Code (LIRIC) (Chaikovsky et al., 2012; Wagner et al., 2013; Granados-Muñoz et al., 2014).

For the analysis of the aerosol hygroscopic properties at the station, specific radiosounding launch campaigns are performed in order to obtain the RH humidity profiles since 2011. Radiosoundings (DFM-09 from GRAW Radiosondes) are launched simultaneously and collocated to the lidar measurements. They provide temperature (resolution 0.01 °C, accuracy 0.2 °C), pressure (resolution 0.1 hPa, accuracy 0.5 hPa), humidity (resolution 1 %, accuracy 2 %) and wind speed (resolution 0.1 m s^{-1}, accuracy

Aerosol hygroscopic growth by active remote sensing and radiosoundings

M. J. Granados-Muñoz et al.

Title Page

Abstract	Introduction
Conclusions	References
Tables	Figures

|◄ | ►|

◄ | ►

Back | Close

Full Screen / Esc

Printer-friendly Version

Interactive Discussion

$0.2\,\mathrm{m\,s}^{-1}$) profiles. Data acquisition and processing are performed by Grawmet5 software and a GS-E ground station from the same manufacturer. GRAW Radiosondes showed good performance at previous intercomparison studies, especially for the RH in the lower troposphere (deviations below 2 %) (Sun et al., 2013).

5 In addition, analysis of backwards trajectories is performed in this study by means of the HYSPLIT model (HYbrid Single-Particle Lagrangian Integrated Trayectory) (Draxler and Rolph, 2003). Day backwards trajectories of air masses arriving at the experimental site at different height levels depending on the region of interest are computed using the model including vertical wind information. The trajectories analysis allows the in-
10 terpretation of the source regions of air masses reaching the experimental site. Under low wind conditions, trajectories have relative error ~ 40 % (Stunder, 1996). The Global Data Assimilation System (GDAS) database is used as input meteorological database for the computations.

3 Methodology

15 ### 3.1 Retrieval of aerosol optical - **microphysical** properties and water vapor **profiles**

From the inversion of the lidar data, the aerosol particle backscatter coefficient profiles (P_λ) are obtained by applying the Klett–Fernald inversion algorithm (Fernald, 1984; Fernald et al., 1972; Klett, 1981, 1985). This algorithm assumes a reference height free of aerosol par-ticles and a height independent aerosol particle lidar ratio (extinction-to-backscatter 20 ratio) for each wavelength. More details can be found in (Bravo-Aranda et al., 2013) and (Guerrero-Rascado et al., 2009, 2011). Aerosol particle lidar ratios assumed when applying the Klett–Fernald algorithm to the lidar data are obtained by minimiz-ing the difference between the integral of the aerosol particle backscatter coefficient profile multiplied by the particle lidar ratio and the aerosol optical depth provided by 25 AERONET for each wavelength (Guerrero-Rascado et al., 2008; Landulfo et al., 2003). The aerosol particle backscatter related Ångström exponent profiles between 355 and

532 nm (β-AE (355–532 nm)), related to the aerosol particles size, are also obtained. In addition, the particle linear depolarization ratio profiles (δ^{P}_{532nm}) are also calculated as explained in (Bravo-Aranda et al., 2013 and references therein) in order to analyse variations in the shape of the particles.

The volume concentration profiles are retrieved by means of Lidar Radiometer Inversion Code (LIRIC). This algorithm provides vertical profiles of microphysical properties from a combined set of sun photometer and lidar data. LIRIC inputs are column-integrated optical and microphysical properties retrieved from the sun photometer measurements using AERONET code (Dubovik et al., 2006) and measured lidar elastic backscatter signals at three different wavelengths (355, 532, and 1064 nm). The depolarization information from lidar data can be optionally used. From this information, the volume concentration profiles for the fine and coarse mode are retrieved (distinguishing between coarse spherical and coarse spheroid particles if depolarization information is considered) (Chaikovsky et al., 2012; Wagner et al., 2013; Granados-Muñoz et al., 2014).

The RH profiles are directly measured by the radiosounding simultaneously and collocated to the lidar measurements, therefore no assumptions concerning the RH profile are needed as in previous studies (Ferrare et al., 1998; Wulfmeyer and Feingold, 2000; Feingold and Morley, 2003).

3.2 Procedure for selection of hygroscopic growth case studies

For the retrieval of the aerosol hygroscopic properties from lidar data, very specific condi-tions need to be fulfilled. Aerosol water uptake is associated to the increase in optical properties such as the aerosol particle backscatter coefficient β^{P}_{λ} and aerosol particle microphysical properties such as the volume concentration. Therefore, for the study of these hygroscopic properties, we need to observe an increase in the aerosol parti-cle backscatter at a certain aerosol layer. This increase has to occur simultaneously to an increase in RH in this aerosol layer in order to consider hygroscopic growth as the possible cause of the changes in the aerosol particle properties. In addition,

a simultaneous decrease of the β-AE and the $\delta^P_{532\,nm}$ is indicative of larger and more spherical particles, which is also clearly related to aerosol hygroscopic growth. To our knowledge, this is the first time that this simultaneous analysis of the β-AE and the $\delta^P_{532\,nm}$ for evaluating hygroscopic growth is presented. This positive correlation be-
5   tween these two aerosol properties usually occur only in cases of aerosol hygroscopic growth or aging processes. Those cases fulfilling the previously described conditions are considered as potential cases of hygroscopic growth.

Once the potential cases of hygroscopic growth are detected, it is necessary to verify that in the analysed aerosol layer the atmospheric particles present a certain degree of 10 homogeneity. In this way, we can corroborate that the variations in the aerosol particle properties such as β^P_λ, β-AE (355–532 nm), $\delta^P_{532\,nm}$ and the volume concentration, are caused by the increase in the aerosol size due to water uptake and not to changes in the aerosol composition or load in the analysed layer. That means that the same aerosol type or mixture must be present along the analysed height range and almost
15   no variations in the aerosol load must exist. For this purpose, ancillary information such as the backward trajectories of the air masses, the potential temperature profiles, θ, or the water vapour mixing ratio profiles, r, are used to ensure that the aerosol layer under study is affected by hygroscopic growth. In this sense, if the origin and the trajectory of the air masses are independent of the altitude in the layer analysed, it is considered
20   that the same aerosol type might have been advected and, therefore, a homogenous aerosol composition might be expected in the analysed layer. Otherwise, variations in the aerosol composition are expected and the case is not considered for analysis of hygroscopic growth. The air mass backward trajectories analyses are mainly used as a first approach selection criterion. In addition, good mixing is required as a bound- 25   ary condition in order to guarantee the homogeneity of the atmospheric aerosol in the investigated layer. In general, constant profiles of θ and r are indicators of well mixed conditions within the atmosphere. In our analysis, θ and r are calculated in the analysed layer to check the mixing conditions. Both atmospheric variables are calculated from the radiosounding temperature and relative humidity profiles. Only those cases

with almost constant values of θ and r in the analysed layer (variations lower than 2° C and $2\,g\,kg^{-1}$ respectively) will be consider for the analysis. Good mixed conditions cannot be guaranteed in any other case.

The backward trajectories analysis and the height independency of r criteria for iden-tifying hygroscopic growth were already used in the study by Veselovskii et al. (2009). However, the height independency of θ is introduced for the first time in this study in order to provide more robust boundary conditions and guarantee the occurrence of hygroscopic growth within a well mixed layer.

If these requirements for the homogeneity on the atmospheric aerosol layer are ful-filled, these cases are selected for a more detailed analysis of atmospheric aerosol hygroscopic properties. For the analysis of the hygroscopic growth, the enhancement factor is defined as:

$$f_\zeta(\mathrm{RH}) = \frac{\zeta(\mathrm{RH})}{\zeta(\mathrm{RH_{ref}})} \tag{1}$$

where $\zeta(\mathrm{RH})$ represents an aerosol property at a certain RH. $\mathrm{RH_{ref}}$ is the so-called reference RH. This $\mathrm{RH_{ref}}$ is chosen as the lowest value of RH in the analysed layer. For this study, $f_\zeta(\mathrm{RH})$ is obtained for β_λ^P profiles ($f_\beta(\mathrm{RH})$) and the volume concentration profiles ($f_{VC}(\mathrm{RH})$).

The enhancement factor total uncertainty is very difficult to determine since it is highly dependent on the uncertainties of the aerosol properties and the RH, on the range of RH considered as well as on the hygroscopic growth of the particle itself and therefore it is not well characterized yet. Adam et al. (2012) provided estimations based on a sensitivity test and Mie calculations. According to their study, this uncertainty varies between 4 % (for RH < 40 %) and 38 % (at RH > 95 %).

For different cases, the ranges of RH and, as a consequence, $\mathrm{RH_{ref}}$ values are dif-ferent. Therefore, in order to make the different results comparable it is necessary to use a common $\mathrm{RH_{ref}}$ value. For this purpose, the Hänel model (Hänel, 1976) is used to parameterize the experimental enhancement factor curves. The general form of the

Hänel equation is expressed as:

$$f_\zeta(\text{RH}) = \left(\frac{1 - \text{RH}}{1 - \text{RH}_\text{ref}}\right)^{-\gamma} \qquad (2)$$

where γ is an indicator of the hygroscopicity of the particles. Larger γ values are related to more hygroscopic aerosol types.

Since atmospheric aerosol hygroscopic properties are highly dependent on the aerosol chemical composition information, NAAPS (Navy Aerosol Analysis and Prediction System) (Christensen, 1997) model is also considered in this study to support the data interpretation with respect to the aerosol type.

Summarizing, for the detection of aerosol hygroscopic growth the following procedure is followed: (1) detection of the aerosol particle backscatter coefficient increase with simultaneous increase in RH in a certain aerosol layer, (2) detection of a simultaneous decrease of the Ångström Exponent and the particle linear depolarization ratio in the same layer (indicators of larger and more spherical particles), (3) confirmation that the atmospheric aerosol layer under study is homogenous. For this purpose, homogeneous boundary conditions are implemented: the origin and the trajectory of the air masses at the analysed layer has to be independent of the altitude and the profiles of r and θ has to be constant with height in this layer as an indicative of well mixed conditions.

4 Results and discussion

Data corresponding to several radiosounding launch campaigns performed at the experimental site during the period 2011 to 2013 were analysed following the methodology described in the previous section. During this period, lidar measurements were always running in coincidence with the radiosounding launches. These lidar measurements have been exhaustively analysed together with the RH profiles provided by the radiosoundings in order to detect cases of aerosol hygroscopic growth. Two case studies corresponding to 22 July 2011 and 22 July 2013 are presented here to

show the potential of the technique described in Sect. 3.2. In these case studies, atmospheric conditions are highly supportive for aerosol hygroscopic growth at certain height ranges. A detailed analysis of these cases is presented in the following paragraphs.

Case I corresponds to the 22 July 2011. On this day, a radiosounding was launched at 20:30 UTC in coincidence with night-time lidar measurements. According to NAAPS model, 22 July 2011 at 18:00 UTC is characterized by the presence of mineral dust above Granada (Fig. S1a in the Supplement). A second case of hygroscopic growth is detected on 22 July 2013 (Case II) during the summer radiosounding campaign. For this specific day, the radiosounding was launched at 20:00 UTC in coincidence with simultaneous lidar measurements. On this day, NAAPS model indicates the presence of sulphates and smoke above the experimental site (Fig. S1b).

Sun photometer experimental data are also used for this analysis, since they provide information about the aerosol properties. In addition, sun photometer data are required for the retrieval of the volume concentration profiles with LIRIC. For Case I, sun photometer data suggest the presence of a Saharan dust plume that dissipates at late afternoon (Fig. 1a). The aerosol optical depth at 440 nm ($\tau_{440\,nm}$) decreases during the afternoon, changing from 0.30 in the morning to values of 0.20 at 18:30 UTC. The Ångström exponent between 440 and 870 nm (AE (440–870 nm)) increases from 0.5 to 1.1, indicating an enhancement in the contribution of fine particles from 15:00 UTC. The aerosol size distributions retrieved during the day also indicate a decrease in the coarse mode and an increase of the fine mode from midday onwards. At 18:30 UTC (Fig. 1b) the aerosol size distributions indicate a balanced presence of both fine and coarse particles. This is confirmed by the fine mode fraction, determined through the SDA (spectral deconvolution algorithm, not shown) (O'Neill et al., 2003) that increases from 0.35 in the early morning up to 0.55 in the late evening. In the retrievals of single scattering albedo, $\varpi(\lambda)$, corresponding to the morning hours it is observed a strong influence of mineral dust (high $\varpi(\lambda)$ values and increasing $\varpi(\lambda)$ with wavelength) (Fig. 1c). However, in the late afternoon, $\varpi(\lambda)$ values around 0.93, and its neutral spectral dependence

suggest the presence in the atmospheric column of aerosol from anthropogenic origin with influence of residual mineral dust (Lyamani et al., 2006a, b; Valenzuela et al., 2012), which will be confirmed later with the lidar data and the backward trajectories analysis (Fig. 1c).

For the second case, $\tau_{440\,nm}$ values indicate high aerosol loads reaching values above 0.40 at 17:19 UTC (Fig. 1d). The AE (440–870 nm) exhibits values larger than 1.2 during the whole day reaching 1.4 at 18:30 UTC, thus indicating a predominance of fine particles. The AERONET inversion retrievals during the whole day show bimodal size distributions with predominance of fine particles (Fig. 1e). Both, the ω (440 nm) values close to 0.9, and their spectral dependence, with a decreasing trend with wavelength, evidence the presence of anthropogenic pollution and/or smoke over Granada (Lyamani et al., 2006a, b) (Fig. 1f), in agreement with NAAPS forecast model.

On both case studies, lidar measurements were running from 20:00 to 22:00 UTC. On 22 July 2011, lidar range corrected signal (RCS) time series (Fig. 2a) indicate the presence of atmospheric aerosol up to 3000 m a.s.l. Moreover, a strong increase of the RCS is observed in the height range around 2400 m a.s.l. between 20:30 and 21:00 UTC. On the other hand, the time series of the lidar RCS on 22 July 2013 (Fig. 2b) indicate that the atmospheric aerosol reach altitudes up to 3500 m a.s.l. with the strongest backscattered lidar signal around 3000 m a.s.l. For this second case, some clouds were observed from 21:30 UTC. The occurrence of these clouds might be related to the ability of hygroscopic aerosol to act as CCN.

The analysis of lidar data by means of the Klett–Fernald inversion algorithm for both cases is shown in Fig. 3. Mean profiles of $\beta^P_{532\,nm}$, β-AE (355–532 nm) and $\delta^P_{532\,nm}$ corresponding to the period 20:30–21:00 UTC for Case I and to 20:00–20:30 UTC for Case II are presented in this figure. On both cases, we observe a marked increase with altitude in $\beta^P_{532\,nm}$, in the range between 1330 and 2330 m a.s.l. for Case I and 1300 and 2700 m a.s.l. for Case II (Fig. 3a). Simultaneous to this increase in $\beta^P_{532\,nm}$, the RH also increases with altitude in both layers (Fig. 3b). Opposite to $\beta^P_{532\,nm}$, β-AE (355–532 nm) decreases with altitude in both layers (Fig. 3c, Table 1). The decrease

in β-AE (355–532 nm) with altitude indicates an increase in aerosol particles size at higher altitudes. The $\delta^P_{532\,nm}$ also decreases with altitude for both cases in the corresponding aerosol layers (Fig. 3d). The positive correlation between β-AE (355–532 nm) and $\delta^P_{532\,nm}$ indicates that the increasing contribution of larger particles corresponds to an increase in particle sphericity, which is a typical behaviour of hygroscopic growth. This positive correlation between β-AE (355–532 nm) and $\delta^P_{532\,nm}$ in cases of hygroscopic growth has never been presented in previous studies. On Case I, $\delta^P_{532\,nm}$ profiles retrieved from lidar data in the analysed aerosol layer are rather low ($\delta^P_{532\,nm} \sim 0.07$), indicating predominance of spherical particles in the analysed layer. However, at higher altitudes $\delta^P_{532\,nm}$ reach values of 0.15 and β-AE (355–532 nm)~ 0.6 with RH values lower than 40 %, indicating that the influence of mineral dust observed in the column with the sun photometer data is more important in this upper layer than in our region of interest.

In order to corroborate that the variations with height in the aerosol properties are due to water uptake and not to inhomogeneities in the aerosol layer, the boundary conditions established in Sect. 3.2 are checked (Fig. 4). The 5-day backward trajectories analysis performed with HYSPLIT model reveals that the origin and trajectories of the air masses are almost identical for the different altitudes within the aerosol layer considered in each case. Therefore, the same aerosol type might have been advected over Granada in the investigated aerosol layers. For Case I, air masses come from the Northwest of Europe, going through the Northern Iberian Peninsula, finally arriving over Granada after overpassing the Iberian Peninsula Mediterranean Coast (Fig. 4a). These air masses might have transported anthropogenic aerosol from Europe to the experimental site, especially considering that they were travelling at very low altitudes, located within the planetary boundary layer according to HYSPLIT retrieved boundary layer heights. The backward trajectories analysis also revealed that the air masses were travelling very close to the sea surface above the Mediterranean Sea and marine aerosols might be probably present in the aerosol mixture (Fig. 4a). For Case II, the air masses come from the Mediterranean region at the three altitude

Aerosol hygroscopic growth by active remote sensing and radiosoundings

M. J. Granados-Muñoz et al.

Title Page

Abstract	Introduction
Conclusions	References
Tables	Figures

◄◄	►►
◄	►
Back	Close

Full Screen / Esc

Printer-friendly Version

Interactive Discussion

levels considered (Fig. 4b) and they were travelling within the marine boundary layer before reaching Granada station, so they are likely loaded with marine aerosol from the Western Mediterranean Sea together with sulphates and smoke from Europe as indicated by the NAAPS model. The trajectories are very similar to those on Case I, but as for this case they travelled more slowly above the Mediterranean Sea they are likely loaded with more marine aerosol than in the previous case.

Vertical profiles of θ and r measured with radiosounding data are also checked in order to corroborate good mixing conditions within the analysed aerosol layers. Both θ and r profiles present almost constant values in the analysed layers in both case studies (Fig. 4c) and thus it can be inferred that the analysed layers are well mixed. Once these conditions are fulfilled, vertical homogeneity in the analysed layers can be assumed. Therefore, hygroscopic growth is foreseen for these cases since there is a high likelihood that changes in the aerosol properties are due to water uptake.

Therefore, according to all the previous results, these cases are considered representative of hygroscopic growth since there is an enhancement in $\beta^P_{532\,nm}$ in coincidence with an increase in RH in the selected aerosol layers. In addition, the positive correlation between the β-AE (355–532 nm) and the $\delta^P_{532\,nm}$ values suggests hygroscopic growth, since aerosol particles become larger and more spherical due to water uptake. Backward trajectories analysis with HYSPLIT and the height independency of θ and r in the analysed height range corroborates that the enhancement of $\beta^{aer}_{532\,nm}$ is due to water uptake because of the homogeneity of the aerosol layer.

Following the methodology described in Sect. 3.2, from the combination of the $\beta^P_{532\,nm}$ and RH profiles in Fig. 3, the aerosol particle backscatter coefficient enhancement factor $f_\beta(RH)$ is obtained as indicated in Eq. (1).

In Case I, $RH_{ref} = 60\%$, which is the lowest value measured in the investigated layer. The dependence of $f_\beta(RH)$ with the RH is shown in the resultant humidogram in Fig. 5a. From this figure, it is evident that $\beta^P_{532\,nm}$ increases 2.5 times ($f_\beta(90\%) = 2.5$) in the range of humidity between 60 and 90 %. The humidogram in Case II (Fig. 5b) shows that $f_\beta(83\%) = 3.5$, in the range of RH between 40 and 83 %. For Case II, RH_{ref} is

established at 40 %, since it is the lowest RH value reached in the analysed layer for this case.

In a similar study performed by Veselovskii et al. (2009) in the East Coast of the United States, they got a value of the aerosol particle extinction coefficient enhancement factor $f_\alpha(85\%) = 2.3$ in the presence of the typical continental haze using $RH_{ref} = 60\%$. It is necessary to take into account that Veselovskii et al. (2009) used the aerosol particle extinction coefficient profile ant thus results are comparable only in a contextual way, since it would be necessary to know the influence of the aerosol hygroscopic growth on the aerosol particle lidar ratio to perform a quantitative comparison. For Case I, the value obtained here for f_β (85 %) is much lower than the one provided by Veselovskii et al. (2009) ($f_\beta(85\%) = 1.5$). However, for Case II $f_\beta(85\%) = 2.6$ using $RH_{ref} = 60\%$, which is very similar to the one obtained by Veselovskii et al. (2009).

A qualitative comparison with in-situ studies can be done in order to contextualize our results. However, when making this comparison it is necessary to take into account the differences between both techniques. In addition, in-situ analyses are usually performed under controlled conditions, whereas lidar data are measured under real and unperturbed conditions. Also, in-situ studies are frequently based on the retrieval of the aerosol particle light-scattering coefficient enhancement factor, $f_\sigma(RH)$, and not on the $f_\beta(RH)$ used here. They usually provide values for $f_\sigma(85\%)$ using RH_{ref} values of 40 % or lower (dry conditions). In order to compare our results to these in-situ studies using a RH_{ref} of 40 %, the Hänel parameterization is applied to our data in Case I (Fig. 5a). For Case II, the Hänel parameterization is necessary to obtain $f_\beta(85\%)$, since RH values above 83 % are not reached. Values of $f_\beta(80\%)$, $f_\beta(85\%)$ using $RH_{ref} = 40\%$ and γ obtained are summarized for both cases in Table 2.

As it can be inferred from Table 2 and Fig. 5, the atmospheric aerosol presents a stronger hygroscopic growth for Case II. According to the experimental AERONET and lidar data and the ancillary information of the model, this may be due to the larger contribution of sulphates (in the fine mode) and marine aerosol (in the coarse mode) during Case II than during Case I in the analysed layers. In addition, a minor influence

Title Page

Abstract | Introduction

Conclusions | References

Tables | Figures

⏮ | ⏭

◀ | ▶

Back | Close

Full Screen / Esc

Printer-friendly Version

Interactive Discussion

of the residual mineral dust particles (which presents very low hygroscopicity) from the morning hours in Case I may have led to low hygroscopic growth of the aerosol mixture (especially for the coarse mode). $f_\beta(80\%)$ values obtained (1.60 ± 0.03 for Case I and 3.00 ± 0.02 for Case II) are in agreement with those presented in Titos et al. (2014a), that range between 1.4 and 3.4, being larger in those cases with marine influence. $f_\beta(85\%)$ (2.10 ± 0.06 for Case I and 3.90 ± 0.03 for Case II) values are similar to those obtained in previous in-situ studies within measurement differences limitations, ranging between 1.2 and 3.4 (Kim et al., 2006; Fierz-Schmidhauser et al., 2010a, b; Adam et al., 2012; Zieger et al., 2013). The γ values obtained from the Hänel parameterization in these case studies are in the range of values obtained in previous studies for the scattering coefficient using tandem of nephelometers (between 0.1 and 1.35) (Raut and Chazette, 2007; Gasso et al., 2000; Randriamiarisoa et al., 2006; Titos et al., 2014a, b).

The availability of the AERONET inversion retrieval data at late afternoon during both cases as shown in Fig. 1 allows us to retrieve volume concentration profiles by means of LIRIC algorithm, assuming no drastic temporal change in aerosol properties between the last AERONET retrieval and lidar measurements (Chaikovsky et al., 2008, 2012; Wagner et al., 2013; Granados-Muñoz et al., 2014). Figure 6a represents these volume concentration profiles obtained by the combination of lidar data from 20:30 to 21:00 UTC and the closest sun photometer retrieval (at 18:30 UTC) on Case I. Figure 6b shows the volume concentration profiles for Case II retrieved from AERONET data at 18:10 UTC and lidar data from 20:00 to 20:30 UTC. As it can be observed, there is a combination of coarse and fine particles along the whole profile for both cases. In both cases, the fine mode volume concentration increases with altitude in both analysed layers. The total volume concentration for Case I increases with height reaching a maximum around 2500 m a.s.l. Figure 6c shows the volume concentration enhancement factor ($f_{VC}(RH)$) for the fine mode and the total volume concentration against RH for Case I. In this case, a threshold value of the volume concentration has been established at $10\,\mu m^3\,cm^{-3}$ since $f_{VC}(RH)$ is a ratio and lower values may

induce a significant overestimation of f_{VC}(RH). Because of this, RH$_{ref}$ for the fine mode is around 73 %. The fine mode volume concentration presents a strong increase with RH, being f_{VC}(80 %) = 1.57. The total volume concentration smoothly increases with RH, mainly due to the increase in the fine mode (f_{VC}(80 %) = 1.16 with RH$_{ref}$ = 60 %).

5   For case II, Fig. 6d shows f_{VC}(RH) vs. RH for the fine mode and the total volume concentration. It is observed an increase of f_{VC}(RH) with RH for the fine mode, slightly smoother than in the previous case, with f_{VC}(80 %) = 1.28. Using RH$_{ref}$ = 60 % in order to make a comparison with Case I, f_{VC}(80 %) for Case II is 1.57 which is larger than in Case I. According to these results, the fine mode is the one dominating the hygro-

10 scopic growth in the analysed layers in both cases. Nonetheless, in Case II there is a larger increase of the total volume concentration with RH than in Case I, indicating that the coarse mode is more hygroscopic for Case II. This can be attributed to the higher influence of the marine aerosol advected from the Mediterranean Sea in the analysed layer in Case II and the minor influence of the residual mineral dust in the

15 analysed layer in Case I, evidencing the influence of the chemical composition on the hygroscopic growth. Larger values of f(RH) are usually obtained for fine mode particles (Di Girolamo et al., 2012; Titos et al., 2014). In our study, it seems that the fine mode is clearly more dominated by more hygroscopic particles whereas the coarse mode is dominated by substances with very low hygroscopic growth, especially for Case I

20 (possible influence of mineral dust in the aerosol mixture). Di Girolamo et al. (2012) observed similar behaviour analysing aged dust particles partially mixed with maritime, urban and organic aerosols. However, according to Zieger et al. (2013), the relative contribution of the fine and the coarse modes and the specific chemical composition for each mode are very important for determining f(RH).

25 **5   Conclusions**

A new methodology to detect aerosol particle hygroscopic growth is implemented at Granada EARLINET experimental site. Aerosol hygroscopic properties are analysed

Aerosol hygroscopic growth by active remote sensing and radiosoundings

M. J. Granados-Muñoz et al.

Title Page

Abstract   Introduction

Conclusions   References

Tables   Figures

|◄   ►|

◄   ►

Back   Close

Full Screen / Esc

Printer-friendly Version

Interactive Discussion

using a multispectral lidar system in combination with radiosounding data obtained during specific campaigns within the period 2011–2013. In the proposed method, an increase of the aerosol particle backscatter coefficient with relative humidity, associated to a decrease in the Ångström exponent and the particle depolarization ratio are used to detect aerosol hygroscopic growth. The positive correlation between the Ångström exponent and the particle linear depolarization ratio is presented here for the first time as an indicator of the aerosol hygroscopic growth. The height independency of the air masses arriving at the station and of the water vapour mixing ratio and the potential temperature profiles are also used as constraints in the method presented here in order to provide more strictness to the identification of the hygroscopic growth cases. The method proved to be reliable for the identification and analysis of hygroscopic growth situations based on the analysis of the aerosol particle properties profiles. The methodology is also applied to the analysis of the hygroscopic growth effects on the volume concentration profiles retrieved by means of LIRIC algorithm, which have never been done before. Two cases of hygroscopic growth within the available dataset (one on 22 July 2011 and another on 22 July 2013) are presented in this study to illustrate the potential of the exposed methodology. Different conditions were observed in these two cases allowing us to analyse the hygroscopic behaviour of different aerosol types. In order to compare the two analysed cases, the Hänel parameterization was used and data were recalculated using a common RH_{ref} value of 40 %. From this comparison, it was observed that the atmospheric aerosol presented a stronger hygroscopic growth during the case study corresponding to 22 July 2013, as indicated by $f_{\beta}(80\%)$, $f_{\beta}(85\%)$ and γ values. This can be explained by the different atmospheric conditions in the two cases. The case corresponding to the 22 July 2011 was affected by a mixture of atmospheric aerosols dominated by anthropogenic pollution and slightly affected by mineral dust and marine aerosol, whereas the case detected on 22 July 2013 was influenced mainly by sulphates with a stronger influence of marine aerosol than Case I, as indicated by AERONET data and the NAAPS model. The values obtained for the backscatter enhancement factor $f_{\beta}(85\%)$ are within the range obtained with in-situ

studies for the case on 22 July 2011, and slightly larger on 22 July 2013. The analysis of the volume concentration profiles reveals an increase of the total volume concentration with relative humidity, dominated in our particular cases by an increase in the fine mode fraction. The increase in the total volume concentration is larger in Case II corresponding to the 22 July 2013, due to the larger influence of the marine aerosol for this case and to the slight influence of mineral dust (non hygroscopic particles) on Case I.

The Supplement related to this article is available online at doi:10.5194/amtd-7-10293-2014-supplement.

References

Adam, M., Putaud, J. P., Martins dos Santos, S., Dell'Acqua, A., and Gruening, C.: Aerosol hygroscopicity at a regional background site (Ispra) in Northern Italy, Atmos. Chem. Phys., 12, 5703–5717, doi:10.5194/acp-12-5703-2012, 2012.

Bravo-Aranda, J. A., Navas-Guzmán, F., Guerrero-Rascado, J. L., Pérez-Ramírez, D., Granados-Muñoz, M. J., and Alados-Arboledas, L.: Analysis of lidar depolarization calibration procedure and application to the atmospheric aerosol characterization, Int. J. Remote. Sens., 34, 3543–3560, 2013.

Chaikovsky, A., Dubovik, O., Goloub, P., Tanre, D., Pappalardo, G., Wandinger, U., Chaikovskaya, L., Denisov, S., Grudo, Y., Lopatsin, A., Karol, Y., Lapyonok, T., Korol, M., Osipenko, F., Savitski, D., Slesar, A., Apituley, A., Arboledas, L. A., Binietoglou, I., Kokkalis, P., Granados Muñoz, M. J., Papayannis, A., Perrone, M. R., Pietruczuk, A., Pisani, G., Rocadenbosch, F., Sicard, M., De Tomasi, F., Wagner, J., and Wang, X.: Algorithm and software for the retrieval of vertical aerosol properties using combined lidar/radiometer data: dissemination in EARLINET, in: 26th International Laser and Radar Conference, Porto Heli, Greece, 2012.

Charlson, R. J., Schwartz, S. E., Hales, J. M., Cess, R. D., Coakley Jr, J. A., Hansen, J. E., and Hofmann, D. J.: Climate forcing by anthropogenic aerosols, Science, 255, 423–430, 1992.

Christensen, J. H.: The Danish Eulerian hemispheric model – a three-dimensional air pollution model used for the Arctic, Atmos. Environ., 31, 4169–4191, 1997.

Covert, D. S., Charlson, R. J., and Ahlquist, N. C.: A study of the relationship of chemical composition and humidity to light scattering by aerosols, J. Appl. Meteorol., 11, 968–976, 1972.

Di Girolamo, P., Summa, D., Bhawar, R., Di Iorio, T., Cacciani, M., Veselovskii, I., Dubovik, O., and Kolgotin, A.: Raman lidar observations of a Saharan dust outbreak event: characterization of the dust optical properties and determination of particle size and microphysical parameters, Atmos. Environ., 50, 66–78, 2012.

Draxler, R. R. and Rolph, G. D.: HYSPLIT (HYbrid Single-Particle Lagrangian Integrated Trajectory) model access via NOAA ARL READY website, available at: http://www.arl.noaa.gov/ready/hysplit4.html (last access: 13 August 2014), NOAA Air Resources Laboratory, Silver Spring, MD, 2003.

Dubovik, O., Holben, B., Eck, T. F., Smirnov, A., Kaufman, Y. J., King, M. D., Tanré, D., and Slutsker, I.: Variability of absorption and optical properties of key aerosol types observed in worldwide locations, J. Atmos. Sci., 59, 590–608, 2002.

Dubovik, O., Sinyuk, A., Lapyonok, T., Holben, B. N., Mishchenko, M., Yang, P., Eck, T. F., Volten, H., Muñoz, O., and Veihelmann, B.: Application of spheroid models to account for

Title Page

Abstract	Introduction
Conclusions	References
Tables	Figures

|◄ | ►|

◄ | ►

Back | Close

Full Screen / Esc

Printer-friendly Version

Interactive Discussion

aerosol particle nonsphericity in remote sensing of desert dust, J. Geophys. Res.-Atmos., 111, D11208, doi:10.1029/2005JD006619, 2006.

Eck, T. F., Holben, B. N., Reid, J. S., Dubovik, O., Smirnov, A., O'Neill, N. T., Slutsker, I., and Kinne, S.: Wavelength dependence of the optical depth of biomass burning, urban, and desert dust aerosols, J. Geophys. Res.-Atmos., 104, 31333–31349, 1999.

Feingold, G. and Morley, B.: Aerosol hygroscopic properties as measured by lidar and comparison with in situ measurements, J. Geophys. Res., 108, 4327, doi:10.1029/2002JD002842, 2003.

Feingold, G., Furrer, R., Pilewskie, P., Remer, L. A., Min, Q., and Jonsson, H.: Aerosol indirect effect studies at Southern Great Plains during the May 2003 intensive operations period, J. Geophys. Res., 111, D05S14, doi:10.1029/2004JD005648, 2006.

Fernald, F. G.: Analysisof atmospheric lidar observations – some comments, Appl. Optics, 23, 652–653, 1984.

Fernald, F. G., Herman, B. M., and Reagan, J. A.: Determination of aerosol height distributions by lidar, J. Appl. Meteorol., 11, 482–489, 1972.

Ferrare, R. A., Melfi, S. H., Whiteman, D. N., Evans, K. D., Poellot, M., and Kaufman, Y. J.: Raman lidar measurements of aerosol extinction and backscattering: 2. Derivation of aerosol real refractive index, single-scattering albedo, and humidification factor using Raman lidar and aircraft size distribution measurements, J. Geophys. Res.-Atmos., 103, 19673–19689, 1998.

Fierz-Schmidhauser, R., Zieger, P., Wehrle, G., Jefferson, A., Ogren, J. A., Baltensperger, U., and Weingartner, E.: Measurement of relative humidity dependent light scattering of aerosols, Atmos. Meas. Tech., 3, 39–50, doi:10.5194/amt-3-39-2010, 2010a.

Fierz-Schmidhauser, R., Zieger, P., Gysel, M., Kammermann, L., DeCarlo, P. F., Baltensperger, U., and Weingartner, E.: Measured and predicted aerosol light scattering enhancement factors at the high alpine site Jungfraujoch, Atmos. Chem. Phys., 10, 2319–2333, doi:10.5194/acp-10-2319-2010, 2010b.

Gasso, S., Hegg, D. A., Covert, D. S., Collins, D., Noone, K. J., Öström, E., Schmid, B., Russell, P. B., Livingston, J. M., and Durkee, P. A.: Influence of humidity on the aerosol scattering coefficient and its effect on the upwelling radiance during ACE-2, Tellus B, 52, 546–567, 2000.

Granados-Muñoz, M. J., Navas-Guzmán, F., Bravo-Aranda, J. A., Guerrero-Rascado, J. L., Lyamani, H., Fernández-Gálvez, J., and Alados-Arboledas, L.: Automatic determination of the

Title Page

Abstract	Introduction
Conclusions	References
Tables	Figures

|◄ | ►|

◄ | ►

Back | Close

Full Screen / Esc

Printer-friendly Version

Interactive Discussion

planetary boundary layer height using lidar: one-year analysis over southeastern Spain, J. Geophys. Res.-Atmos., 117, D18208, doi:10.1029/2012JD017524, 2012.

Granados-Muñoz, M. J., Guerrero-Rascado, J. L., Bravo-Aranda, J. A., Navas-Guzmán, F., Valenzuela, A., Lyamani, H., Chaikovsky, A., Wandinger, U., Ansmann, A., Dubovik, O., Grudo, J. O., and Alados-Arboledas, L.: Retrieving aerosol microphysical properties by Lidar-Radiometer Inversion Code (LIRIC) for different aerosol types, J. Geophys. Res.-Atmos., 119, 4836–4858, 2014.

Guerrero-Rascado, J. L., Ruiz, B., and Alados-Arboledas, L.: Multi-spectral Lidar characterization of the vertical structure of Saharan dust aerosol over southern Spain, Atmos. Environ., 42, 2668–2681, 2008.

Guerrero-Rascado, J. L., Olmo, F. J., Avilés-Rodríguez, I., Navas-Guzmán, F., Pérez-Ramírez, D., Lyamani, H., and Alados Arboledas, L.: Extreme Saharan dust event over the southern Iberian Peninsula in september 2007: active and passive remote sensing from surface and satellite, Atmos. Chem. Phys., 9, 8453–8469, doi:10.5194/acp-9-8453-2009, 2009.

Guerrero-Rascado, J. L., Andrey, J., Sicard, M., Molero, F., Comerón, A., Pujadas, M., and Alados-Arboledas, L.: Aerosol closure study by lidar, Sun photometry, and airborne optical counters during DAMOCLES field campaign at El Arenosillo sounding station, Spain, J. Geophys. Res.-Atmos., 116, D02209, doi:10.1029/2010JD014510, 2011.

Hänel, G.: The properties of atmospheric aerosol particles as functions of the relative humidity at thermodynamic equilibrium with the surrounding moist air, in: Advances in Geophysics, edited by: Landsberg, H. E. and Mieghem, J. V., Elsevier, 73–188, 1976.

Hegg, D. A., Covert, D. S., Rood, M. J., and Hobbs, P. V.: Measurements of aerosol optical properties in marine air, J. Geophys. Res.-Atmos., 101, 12893–12903, 1996.

Holben, B. N., Eck, T. F., Slutsker, I., Tanré, D., Buis, J. P., Setzer, A., Vermote, E., Reagan, J. A., Daufman, Y. J., Nakajima, T., Lavenu, F., Jankowiak, I., and Smirnov, A.: AERONET – a federated instrument network and data archive for aerosol characterization, Remote Sens. Environ., 66, 1–16, 1998.

IPCC: Contribution of Working Group I to the Fifth Assessment Report of the Intergovernmental Panel on Climate Change, in: Summary for Policymakers in Climate Change, edited by: Stocker, T. F., Qin, D., Plattner, G. K., Tignor, M., Allen, S., Boschung, J., Nauels, A., Xia, Y., Bex, V., and Midgley, P., Cambridge University Press, 2013.

Title Page

Abstract | Introduction

Conclusions | References

Tables | Figures

|◄ | ►|

◄ | ►

Back | Close

Full Screen / Esc

Printer-friendly Version

Interactive Discussion

Kim, J., Yoon, S. C., Jefferson, A., and Kim, S. W.: Aerosol hygroscopic properties during Asian dust, pollution, and biomass burning episodes at Gosan, Korea in April 2001, Atmos. Environ., 40, 1550–1560, 2006.

Klett, J. D.: Stableanalytical inversion solution for processing lidar returns, Appl. Optics, 20, 211–220, 1981.

Klett, J. D.: Lidarinversion with variable backscatter/extinction ratios, Appl. Optics, 24, 1638–1643, 1985.

Landulfo, E., Papayannis, A., Artaxo, P., Castanho, A. D. A., de Freitas, A. Z., Souza, R. F., Vieira Junior, N. D., Jorge, M. P. M. P., Sánchez-Ccoyllo, O. R., and Moreira, D. S.: Synergetic measurements of aerosols over São Paulo, Brazil using LIDAR, sunphotometer and satellite data during the dry season, Atmos. Chem. Phys., 3, 1523–1539, doi:10.5194/acp-3-1523-2003, 2003.

Lyamani, H., Olmo, F. J., Alcántara, A., and Alados-Arboledas, L.: Atmospheric aerosols during the 2003 heat wave in southeastern Spain I: spectral optical depth, Atmos. Environ., 40, 6453–6464, 2006a.

Lyamani, H., Olmo, F. J., Alcántara, A., and Alados-Arboledas, L.: Atmospheric aerosols during the 2003 heat wave in southeastern Spain II: microphysical columnar properties and radiative forcing, Atmos. Environ., 40, 6465–6476, 2006b.

Massling, A., Leinert, S., Wiedensohler, A., and Covert, D.: Hygroscopic growth of sub-micrometer and one-micrometer aerosol particles measured during ACE-Asia, Atmos. Chem. Phys., 7, 3249–3259, doi:10.5194/acp-7-3249-2007, 2007.

Navas-Guzmán, F., Bravo-Aranda, J. A., Guerrero-Rascado, J. L., Granados-Muñoz, M. J., and Alados-Arboledas, L.: Statistical analysis of aerosol optical properties retrieved by Raman lidar over Southeastern Spain, Tellus B, 65, 21234, doi:10.3402/tellusb.v65i0.21234, 2013.

Navas-Guzmán, F., Fernández-Gálvez, J., Granados-Muñoz, M. J., Guerrero-Rascado, J. L., Bravo-Aranda, J. A., and Alados-Arboledas, L.: Tropospheric water vapour and relative humidity profiles from lidar and microwave radiometry, Atmos. Meas. Tech., 7, 1201–1211, doi:10.5194/amt-7-1201-2014, 2014.

O'Neill, N. T., Eck, T. F., Smirnov, A., Holben, B. N., and Thulasirama, S.: Spectral discrimination of coarse and fine mode optical depth, J. Geophys. Res., 108, 4559, doi:10.1029/2002JD002975, 2003.

Pahlow, M., Feingold, G., Jefferson, A., Andrews, E., Ogren, J. A., Wang, J., and Turner, D. D.: Comparison between lidar and nephelometer measurements of aerosol hygroscopicity at the

Aerosol hygroscopic growth by active remote sensing and radiosoundings

M. J. Granados-Muñoz et al.

Title Page

Abstract | Introduction

Conclusions | References

Tables | Figures

Back | Close

Full Screen / Esc

Printer-friendly Version

Interactive Discussion

Southern Great Plains Atmospheric Radiation Measurement site, J. Geophys. Res.-Atmos., 111, D05S15, doi:10.1029/2004JD005646, 2006.

Pappalardo, G., Amodeo, A., Pandolfi, M., Wandinger, U., Ansmann, A., Bösenberg, J., Matthias, V., Amiridis, V., De Tomasi, F., Frioud, M., Iarlori, M., Komguem, L., Papayannis, A., Rocadenbosch, F., and Wang, X.: Aerosol lidar intercomparison in the framework of the EARLINET project. 3. Raman lidar algorithm for aerosol extinction, backscatter, and lidar ratio, Appl. Optics, 43, 5370–5385, 2004.

Pappalardo, G., Amodeo, A., Apituley, A., Comeron, A., Freudenthaler, V., Linné, H., Ansmann, A., Bösenberg, J., D'Amico, G., Mattis, I., Mona, L., Wandinger, U., Amiridis, V., Alados-Arboledas, L., Nicolae, D., and Wiegner, M.: EARLINET: towards an advanced sustainable European aerosol lidar network, Atmos. Meas. Tech., 7, 2389–2409, doi:10.5194/amt-7-2389-2014, 2014.

Randriamiarisoa, H., Chazette, P., Couvert, P., Sanak, J., and Mégie, G.: Relative humidity impact on aerosol parameters in a Paris suburban area, Atmos. Chem. Phys., 6, 1389–1407, doi:10.5194/acp-6-1389-2006, 2006.

Raut, J.-C. and Chazette, P.: Retrieval of aerosol complex refractive index from a synergy between lidar, sunphotometer and in situ measurements during LISAIR experiment, Atmos. Chem. Phys., 7, 2797–2815, doi:10.5194/acp-7-2797-2007, 2007.

Stunder, B. J. B.: Anassessment of the quality of forecast trajectories, J. Appl. Meteorol., 35, 1319–1331, 1996.

Sun, B., Reale, A., Schroeder, S., Seidel, D. J., and Ballish, B.: Toward improved corrections for radiationinduced biases in radiosonde temperature observations, J. Geophys. Res.-Atmos., 118, 4231–4243, 2013.

Titos, G., Foyo-Moreno, I., Lyamani, H., Querol, X., Alastuey, A., and Alados-Arboledas, L.: Optical properties and chemical composition of aerosol particles at an urban location: an estimation of the aerosol mass scattering and absorption efficiencies, J. Geophys. Res.-Atmos., 117, D04206, doi:10.1029/2011JD016671, 2012.

Titos, G., Jefferson, A., Sheridan, P. J., Andrews, E., Lyamani, H., Alados-Arboledas, L., and Ogren, J. A.: Aerosol light-scattering enhancement due to water uptake during the TCAP campaign, Atmos. Chem. Phys., 14, 7031–7043, doi:10.5194/acp-14-7031-2014, 2014a.

Titos, G., Lyamani, H., Pandolfi, M., Alastuey, A., and Alados-Arboledas, L.: Identification of fine (PM_1) and coarse (PM_{10-1}) sources of particulate matter in an urban environment, Atmos. Environ., 89, 593–602, 2014b.

Title Page

Abstract | Introduction

Conclusions | References

Tables | Figures

◀◀ | ▶▶

◀ | ▶

Back | Close

Full Screen / Esc

Printer-friendly Version

Interactive Discussion

Titos, G., Lyamani, H., Cazorla, A., Sorribas, M., Foyo-Moreno, I., Wiedensohler, A., and Alados-Arboledas, L.: Study of the relative humidity dependence of aerosol light-scattering in southern Spain, Tellus B, 66, 24536, doi:10.3402/tellusb.v66.24536, 2014c.

Valenzuela, A., Olmo, F. J., Lyamani, H., Antón, M., Quirantes, A., and Alados-Arboledas, L.: Classification of aerosol radiative properties during African desert dust intrusions over south-eastern Spain by sector origins and cluster analysis, J. Geophys. Res.-Atmos., 117, D06214, doi:10.1029/2011JD016885, 2012.

Veselovskii, I., Whiteman, D. N., Kolgotin, A., Andrews, E., and Korenskii, M.: Demonstration of aerosol property profiling by multiwavelength lidar under varying relative humidity conditions, J. Atmos. Ocean. Tech., 26, 1543–1557, 2009.

Wagner, J., Ansmann, A., Wandinger, U., Seifert, P., Schwarz, A., Tesche, M., Chaikovsky, A., and Dubovik, O.: Evaluation of the Lidar/Radiometer Inversion Code (LIRIC) to determine microphysical properties of volcanic and desert dust, Atmos. Meas. Tech., 6, 1707–1724, doi:10.5194/amt-6-1707-2013, 2013.

Wu, Z., Birmili, W., Poulain, L., Wang, Z., Merkel, M., Fahlbusch, B., van Pinxteren, D., Herrmann, H., and Wiedensohler, A.: Particle hygroscopicity during atmospheric new particle formation events: implications for the chemical species contributing to particle growth, Atmos. Chem. Phys., 13, 6637–6646, doi:10.5194/acp-13-6637-2013, 2013.

Wulfmeyer, V. and Feingold, G.: On the relationship between relative humidity and particle backscattering coefficient in the marine boundary layer determined with differential absorption lidar, J. Geophys. Res.-Atmos., 105, 4729–4741, 2000.

Zieger, P., Fierz-Schmidhauser, R., Weingartner, E., and Baltensperger, U.: Effects of relative humidity on aerosol light scattering: results from different European sites, Atmos. Chem. Phys., 13, 10609–10631, doi:10.5194/acp-13-10609-2013, 2013.

Title Page

Abstract	Introduction
Conclusions	References
Tables	Figures

|◄ | ►|

◄ | ►

Back | Close

Full Screen / Esc

Printer-friendly Version

Interactive Discussion

Table 1. Values of the different aerosol properties at the lowest and highest altitudes of the analysed layers for Case I and Case II.

	Case I		Case II	
	1330 m a.s.l.	2330 m a.s.l.	1300 m a.s.l.	2700 m a.s.l.
$\beta_{532\,nm}^{par}$ (Mm^{-1} sr^{-1})	2.17	4.20	1.11	3.84
RH (%)	60	90	40	85
β-AE (355–532 nm)	1.3	0.8	2.0	1.0
$\delta_{532\,nm}^{P}$	0.10	0.05	0.07	0.03

Table 2. Values of $f_\beta(80\%)$, $f_\beta(85\%)$ and γ for the two cases of hygroscopic growth corresponding to the 22 July of 2011 and 2013, respectively. The uncertainties in $f_\beta(\mathrm{RH})$ are obtained by error propagation applied to Eq. (1). Only the uncertainty introduced by the aerosol particle backscatter coefficient is considered.

	Case I	Case II
$f_\beta(80\%)$	1.60 ± 0.03	3.00 ± 0.02
γ	0.56 ± 0.01	1.07 ± 0.01
$f_\beta(85\%)$	2.10 ± 0.06	3.90 ± 0.03
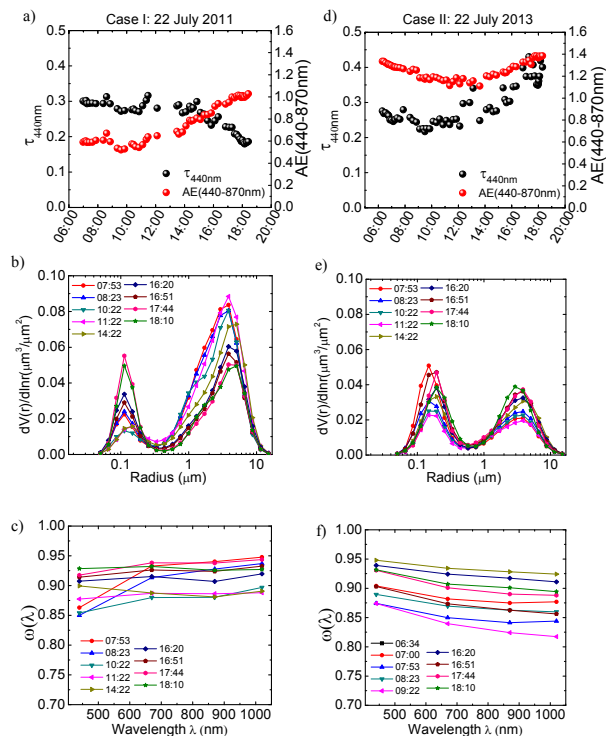
Figure 1. (a) AERONET τ_{440} and AE (440–870) daily time series for Case I. **(b)** AERONET retrieved volume size distributions for Case I. **(c)** $\varpi(\lambda)$ for Case I. **(d)** AERONET τ_{440} and AE (440–870) daily time series for Case II. **(e)** AERONET retrieved volume size distributions for Case II. **(f)** $\varpi(\lambda)$ for Case II.
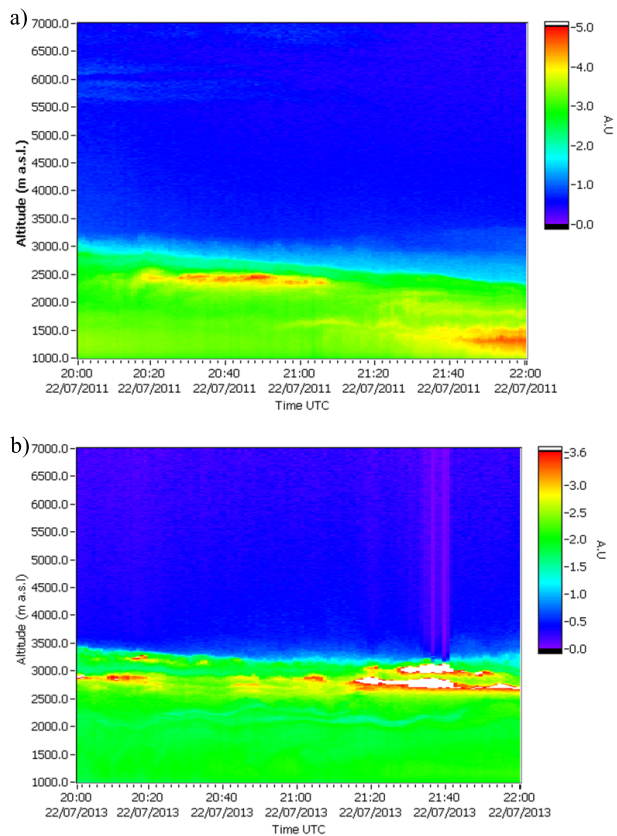
Figure 2. (a) Lidar RCS time series at 532 nm (arbitrary units) on 22 July 2011 from 20:00 to 22:00 UTC **(b)** Lidar RCS time series at 532 nm (arbitrary units) on 22 July 2013 from 20:00 to 22:00 UTC.
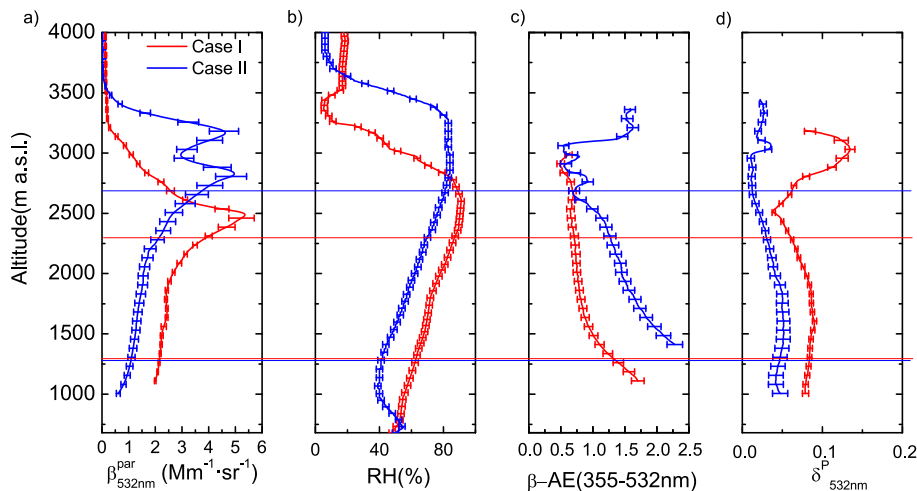
Figure 3. (a) $\beta^{P}_{532\,nm}$ retrieved with Klett–Fernald algorithm (LR = 65 sr for Case I and LR = 70 for Case II) from 20:30 to 21:00 UTC on Case I and 20:00 to 20:30 UTC on Case II **(b)** RH profiles from the radiosounding launched at 20:30 UTC on Case I and at 20:00 UTC on Case II. **(c)** β-AE (355–532 nm) retrieved with Klett–Fernald algorithm for the same periods. **(d)** $\delta^{P}_{532\,nm}$ retrieved from lidar data for the same periods. The error bars indicate the uncertainties calculated by Monte-Carlo technique. Horizontal lines represent the height limits of the aerosol layers selected for the analysis in Case I (red line) and Case II (blue lines).
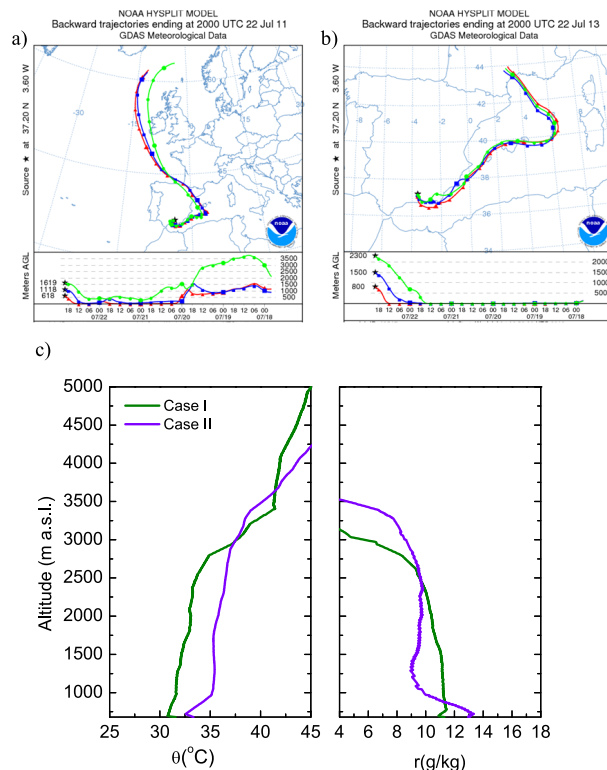
Figure 4. (a) 5-day backtrajectories of the air masses ending on 22 July 2011 at 20:00 UTC at Granada at 3 altitude heights within 1330–2330 m a.s.l. height range. **(b)** 5 day backtrajectories of the air masses ending on 22 July 2013 at 20:00 UTC at at Granada at 3 altitude heights within 1300–2700 m a.s.l. height range. **(c)** Vertical profiles of θ (in °C) and r (in g kg^{-1}) from radiosounding data on 22 July 2011 at 20:30 UTC (Case I) and 22 July 2013 at 20:00 UTC (Case II).
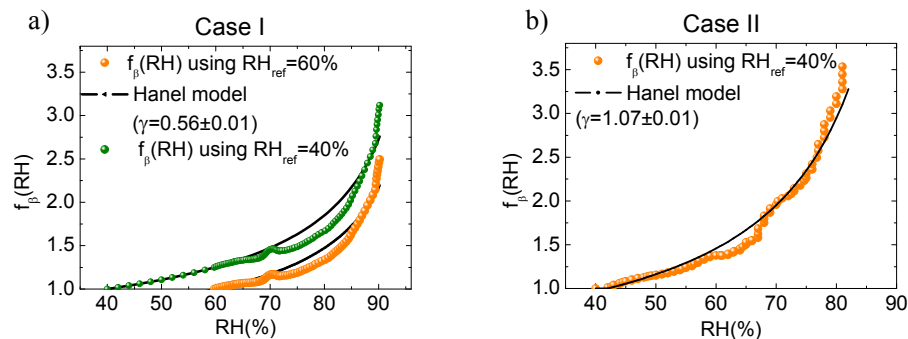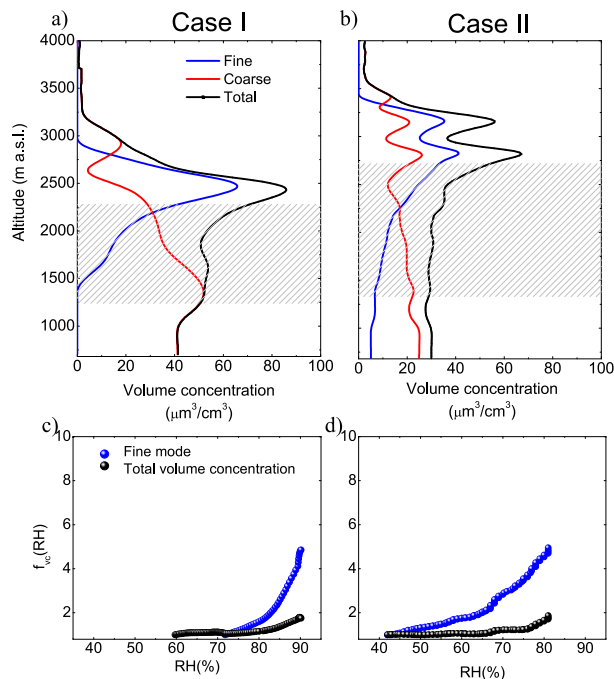
Figure 5. (a) f_β(RH) retrieved on 22 July 2011 (Case I) from 20:30 to 21:00 UTC for the height range between 1330 and 2330 m a.s.l. (yellow dots for $RH_{ref} = 60\%$ and green dots for $RH_{ref} = 40\%$). **(b)** f_β(RH) retrieved on 22 July 2013 (Case II) from 20:00 to 20:30 UTC for the layer corresponding to heights between 1300 and 2700 m a.s.l. using $RH_{ref} = 40\%$.

Figure 6. (a) LIRIC retrieved volume concentration (fine mode, coarse mode and total volume concentration) profiles on 22 July 2011 from 20:30 to 21:00 UTC. The shaded area indicates the height range where hygroscopic growth was investigated. **(b)** LIRIC retrieved volume concentration profiles on 22 July 2013 from 20:00 to 20:30 UTC. The shaded area indicates the investigated height range. **(c)** f_{VC}(RH) vs. RH for the fine mode and the total volume concentrations for 22 July 2011 and the layer corresponding to heights between 1330 and 2330 m a.s.l. **(d)** f_{VC}(RH) vs. RH for the fine mode and the total volume concentrations for 22 July 2013 and the layer corresponding to heights between 1300 and 2700 m a.s.l.